High-temperature superconductivity in the Ca-Sc-H system

D. A. Papaconstantopoulos*
Department of Computational and Data Sciences, George Mason University, Fairfax, Virginia 22030, USA

M. J. Mehl†
Center for Materials Genomics, Duke University, Durham, North Carolina 27708, USA

E. N. Economou‡
Foundation for Research and Technology - Hellas (FORTH), 100 N. Plastira Str., Vasilika Vouton, 700 13 Heraklion Crete, Greece

(Received 18 August 2023; revised 2 November 2023; accepted 14 November 2023; published 8 December 2023)

The discovery of high critical temperature T_c in compressed H_3S has been followed by the prediction and experimental confirmation of even higher superconducting temperatures with T_c approaching room temperature in LaH_{10} and CaH_6. These works established the mechanism of the electron-phonon interaction and the dominant role of hydrogen in these materials. In the present work we focus on CaH_6 and we follow the classic McMillan paper, which writes the electron-phonon coupling parameter λ as a ratio of an electronic contribution η over a force constant $k = M\langle\omega^2\rangle$ which contains the phonon contribution. First the numerator of McMillan's expression, the Hopfield-McMillan parameter η, is computed using the theory of Gaspari and Gyorffy (GG), and the force constants in the denominator are obtained from the paper of Quan *et al.* The resulting λ is used in the Allen-Dynes equation to calculate T_c. We present an analysis of the different terms of the GG equation and conclude that the sp channel of hydrogen has the most important contribution to obtain high values of T_c, as in the other hydrogenated materials. In addition, we further separate the three terms of the GG expression and assess the role of the phase shifts term versus the partial densities of states and free scatterers. We compare these quantities in CaH_6 to those in SH_3 and LaH_{10} and, in contrast to what is expected for high values of λ, we conclude that in CaH_6 the coupling parameter λ is the better indicator of high T_c than η. However, we have found that in the strong coupling limit of large λ the high values of T_c are strongly dependent on the parameter η and make T_c a decreasing function of η. Unfortunately most of the researchers of these materials have ignored the importance of the parameter η partly because the computational packages they are using do not separately compute η. Our view is that the parameters η, κ, and λ must be examined on an equal footing as we study how to achieve high T_c at low pressures. Finally, we present the following findings: (a) using the virtual crystal approximation and an extension of the Allen-Dynes finding that at the strong coupling limit T_c depends on η, we predict that the alloy $Ca_{1-x}Sc_xH_6$ can reach higher T_c than CaH_6. (b) If the higher hydrogen content material CaH_{10} can be made in the $Fm\bar{3}m$ structure it would have significantly higher T_c than CaH_6.

DOI: 10.1103/PhysRevB.108.224508

I. INTRODUCTION

The prediction of high-temperature superconductivity at about 200 K by Duan *et al.* [1] at extreme pressures above 200 GPa in H_3S in the $Im\bar{3}m$ crystal structure [2]. and the experimental confirmation by Drozdov *et al.* [3], were followed by the discovery of high-temperature superconductivity under high pressure in several other hydrides, prominent of which are LaH_{10} and CaH_6 [4–17]. The consensus is that conventional BCS electron-phonon coupling is the operating mechanism. Prominent among the high-temperature superhydrides under pressure is the near room temperature (RT) superconductivity prediction of Liu *et al.* [7,15] for LaH_{10}. After the prediction of Liu *et al.*, experimental papers by Somayazulu *et al.* [18] and Drozdov *et al.* [15] confirmed superconductivity with T_c over 250 K in LaH_{10}.

The idea of metallization of hydrogen was first proposed long ago by Wigner and Huntington [19], and Ashcroft [20] later predicted RT superconductivity in metallic hydrogen under extreme pressures. After Ashcroft's prediction, Papaconstantopoulos and Klein [21] used the Gaspari-Gyorffy (GG) theory [22] to calculate electron-phonon coupling $\lambda = 1.86$ and superconducting temperature $T_c = 234$ K at a pressure of 460 GPa for metallic hydrogen. Unfortunately, metallization of pure hydrogen requires a pressure as high as 500 GPa [23]. The metal hydrides are thus an interesting alternative since they form metallic-like states at much lower pressures.

A special characteristic of the hydrides is the separation of the acoustic and optical phonon modes. The role of the

*dpapacon@gmu.edu
†michael.mehl@duke.edu
‡economou@admin.forth.gr

metallic element (e.g., S or La) is to stabilize the material in a particular structure, but it is the hydrogen metallic-like states which are responsible for superconductivity [24]. Another high-temperature superconductor is CaH_6, the subject of the present work. CaH_6 was first suggested as a high T_c material by Wang *et al.* [25] More recently Ma *et al.* [26] and Li *et al.* [27] synthesized this material and measured T_c in the range 207–215 K and corresponding pressures of 170–181 GPa. In addition, computational studies were presented by Quan *et al.* [28] and by Jeon *et al.* [29]. In the present work on CaH_6 we use linearized augmented plane wave (LAPW) derived electronic density of states (DOS) and wave functions and the GG theory to calculate the parameter η. This parameter, divided by the force constant $k = M\langle\omega^2\rangle$, with phonon frequencies from Quan *et al.*, determines the electron-phonon coupling λ and T_c. We previously used the same procedure [16,30] to calculate η in SH_3 and LaH_{10} stressing the importance of calculating directly the parameter η. In this work we present additional evidence on the usefulness of carefully examining η and not only relying on the value of λ. Calculations of the parameter η across the periodic table are given in a recent book [31].

II. COMPUTATIONAL DETAILS

Superconducting CaH_6 has a clathrate structure with $Im\bar{3}m$ symmetry [25]. The electronic structure calculations were performed with the all-electron linearized augmented plane wave (LAPW) method [32], specifically the Wei-Krakauer-Singh code [33] developed at the U.S. Naval Research Laboratory. The present calculations use the Hedin-Lundqvist form of the local density approximation [34]. We set $RK_{\max} = 8.0$, and the muffin-tin radii $R_{\rm Ca} = 1.8$ bohr and $R_{\rm H} = 1.0$ bohr. Local orbitals were used for the Ca site. To ensure sufficient accuracy for convergence, the total and orbital-projected densities of electronic states (pDOS) are calculated by the tetrahedron method with a uniformly distributed k-point grid of 285 k points in the bcc irreducible Brillouin zone.

The key step to estimate T_c is the determination of the electron-phonon coupling λ, which, as pointed out by McMillan [35] and Hopfield [36], can be written as

$$\lambda_j = \frac{\eta_j}{M_j\langle\omega_j^2\rangle} = \frac{N(\varepsilon_F)\langle I_j^2\rangle}{M_j\langle\omega_j^2\rangle}, \tag{1}$$

where $N(\varepsilon_F)$ is the total DOS per spin at the Fermi level ε_F, $\langle I_j^2\rangle$ is the electron-ion matrix element, $\langle\omega_j^2\rangle$ is the average phonon frequency, and the index j corresponds to calcium or hydrogen. The Hopfield parameter η_j, which only describes electronic properties, is calculated using the GG formula based on scattering theory. This formula allows us to express the electronic contributions to the λ_j in local terms in the following form:

$$\eta_j = \frac{1}{N(\varepsilon_F)}\sum_{\ell=0}^{2} 2(\ell+1)\sin^2\left(\delta_\ell^j - \delta_{\ell+1}^j\right)v_\ell^j v_{\ell+1}^j. \tag{2}$$

$v_\ell^j = N_\ell^j(\epsilon_F)/N_\ell^{j(1)}$ is the ratio of the partial DOS to the free scatterer DOS. Both δ and v are orbital ℓ and site j dependent. The phase shifts δ_ℓ^j are defined through the following equation:

$$\tan\delta(R_s,\varepsilon_F) = \frac{j_\ell' - j_\ell(kR_s)L_\ell(R_s,\varepsilon_F)}{n_\ell' - n_\ell(kR_s)L_\ell(R_s,\varepsilon_F)}, \tag{3}$$

where $k = \sqrt{\varepsilon_F}$ in atomic units, $L_\ell = u_\ell'/u_\ell$ is the logarithmic derivative, and j_ℓ and n_ℓ are spherical Bessel and Neumann functions. The free scatterer DOS $N_\ell^{j(1)}$ is defined as follows:

$$N_\ell^{j(1)} = (2\ell+1)\int_0^{R^{\rm MT}}\left[u_\ell^j(r,\varepsilon_F)\right]^2 r^2 dr, \tag{4}$$

where u_ℓ is the radial wave function and the upper limit of the integral is the muffin-tin radius $R^{\rm MT}$ for each atom.

Finally, T_c is evaluated using the Allen-Dynes equation [37] as follows:

$$T_c = f_1 f_2 \frac{\omega_{\log}}{1.2}\exp\left[-\frac{1.04(1+\lambda)}{\lambda - \mu^\star(1+0.62\lambda)}\right], \tag{5}$$

with λ being the sum of the individual atomic values:

$$\lambda = \lambda_{\rm Ca} + 6\lambda_{\rm H}. \tag{6}$$

Here $\lambda_{\rm Ca}$ represents the acoustic modes associated with the calcium atom, and $\lambda_{\rm H}$ is the contribution from the optical modes of hydrogen atoms. This separation is exact for these materials and was pointed out for other hydrides [38]. We have set the Coulomb pseudopotential $\mu^* = 0.13$. f_1 is the strong coupling factor,

$$f_1 = \left[1 + \left(\frac{\lambda}{2.46 + 9.35\mu^\star}\right)^{1.5}\right]^{1/3}, \tag{7}$$

and f_2 is the "shape correction" of Allen and Dynes [37]:

$$f_2 = 1 + \left(\frac{\langle\omega\rangle({\rm H})}{\omega_{\log}} - 1\right)\frac{\lambda^2}{\lambda^2 + Y^2}, \tag{8}$$

where

$$Y = 1.82(1+6.3\mu^*)\frac{\langle\omega\rangle({\rm H})}{\omega_{\log}}. \tag{9}$$

III. RESULTS AND ANALYSIS

Figure 1 shows the energy and pressure versus volume behavior for CaH_6, calculated using code VASP [39–42]. This was performed as validation of our LAPW results. Zero pressure corresponds to an equilibrium volume of 256.0 bohr^3 per unit cell or a lattice parameter $a = 8.0$ bohr, which is in perfect agreement between VASP and our LAPW calculations. At pressures above the solid black line of Fig. 1 the structure is mechanically stable. We also used the AFLOW (Automatic Flow) Automatic Phonon Library (APL) module [43–45] and VASP to calculate the phonon dispersion curves for various lattice constants and found that CaH_6 is stable for lattice constants smaller than 6.88 bohr, corresponding to pressures larger than 95 GPa, where stability is defined by the entire phonon spectrum showing no imaginary frequencies. This is demonstrated in Fig. 2 where for $a = 6.9$ bohr the material shows imaginary frequencies near the symmetry point H, and is thus unstable while $a = 6.8$ is stable.

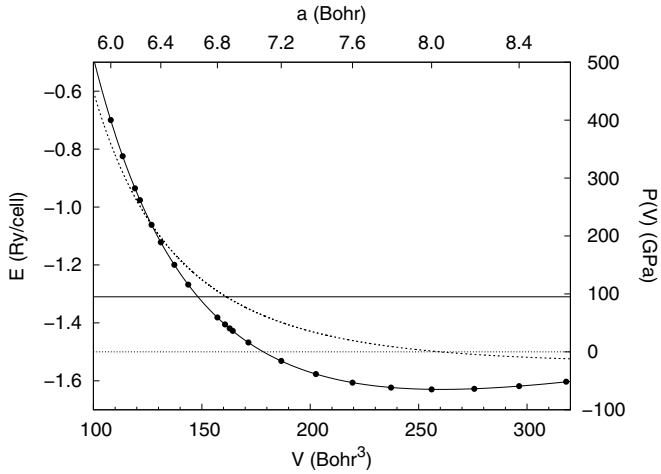

FIG. 1. Energy (solid line with points) and pressure (dotted line) versus volume for CaH_6 using the LDA. Energies were calculated using VASP, while the curves are from a third-order Birch fit to $E(V)$. At pressures above the solid black line the structure is mechanically stable.

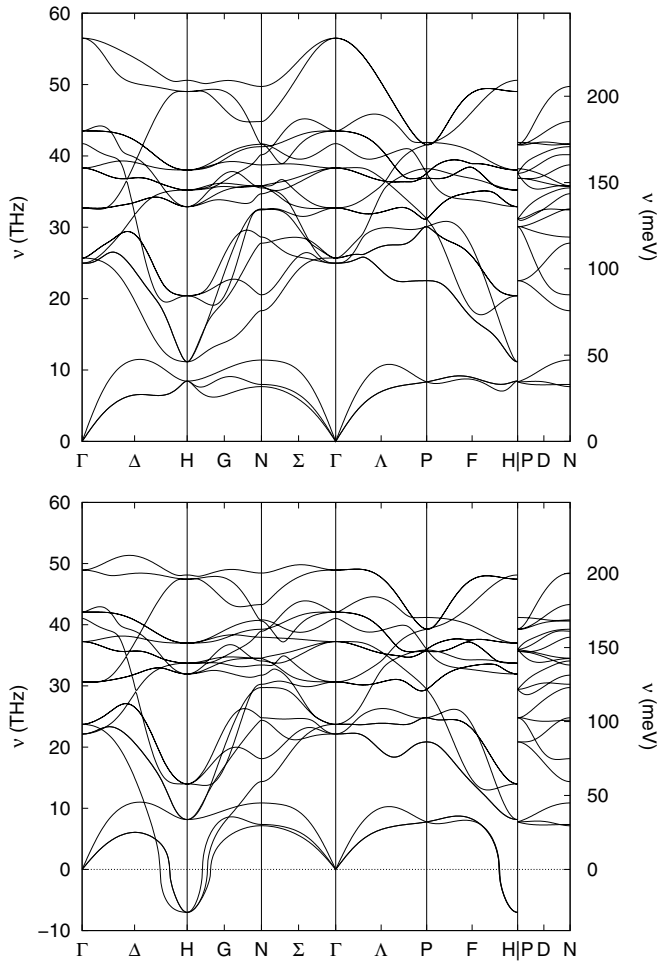

FIG. 2. Phonon frequencies for CaH_6 at 6.8 (top) and 6.9 bohr (bottom), using the AFLOW APL module [43–45]. Imaginary frequencies are plotted on the negative y axis in these graphs.

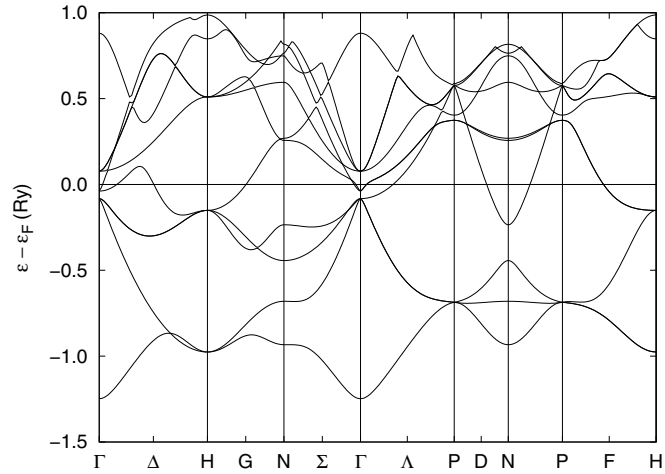

FIG. 3. Band structure of CaH_6 at the lattice constant $a = 6.4$ bohr, corresponding to a pressure of 197.0 GPa. We have shifted the energy scale so that the Fermi level is at zero. Calculations were performed with the LAPW code as described in the text.

In Figs. 3 and 4 we show the energy bands and densities of states for CaH_6 at the lattice constant $a = 6.4$ bohr or pressure $P = 197$ GPa. Comparing these two graphs with those of Quan *et al.* [28] and of Jeon *et al.* [29] we generally find very good agreement. Small differences cannot be detected due the different format of the figures. All papers show metallic

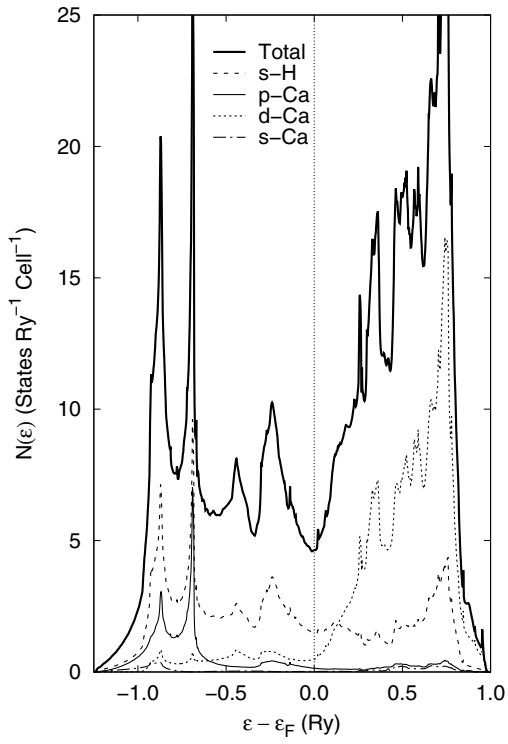

FIG. 4. Total and angular-momentum decomposed electronic density of states for CaH_6, $a = 6.4$ bohr, corresponding to a pressure of 197 GPa. We have shifted the energy scale so that the Fermi level is at zero. Calculations were performed with the LAPW code as described in the text.

behavior and project very similar Fermi surfaces and occupied band widths of approximately 20 eV. Interestingly, the DOS plot shows that the Fermi level falls at a minimum. This is different from SH_3 and LaH_{10} where ε_F lies very close to a van Hove singularity at similar pressures. Since the DOS above ε_F in CaH_6 increases rapidly, a rigid band model would suggest that alloying with Sc would increase $N(\varepsilon_F)$ and create the conditions of a higher T_c in a Ca-Sc-H_6 compound. We will return to this point later. In Fig. 4 we plot the site and angular momentum decomposed DOS for CaH_6 at a lattice constant of 6.4 bohr. We note that the strongest overall contribution comes from the six H *s* sites and the second strongest from the Ca *d* states near ε_F, which dominates the DOS above ε_F. The strong contribution of the *d* states at ε_F is in agreement with Jeon *et al.* but in disagreement with Quan *et al.* who probably used a pseudopotential neglecting the *d* states.

We have shown that the *d*-like contribution of Ca in the DOS at E_f is larger than the per site *s*-like contribution of H. There is nothing strange about this result and it is in agreement with Jeon *et al.* [29], who explained it as hybridization of *s*-H and *d*-Ca states. We have further investigated this point by performing new calculations using different band structure methods and codes, i.e., ELK, VASP, QE, and a tight-binding (TB) fit that we did using our LAPW results. In Appendix A we present a table that shows the following: The results from ELK and our LAPW code agree very well, and give the inside-the-spheres DOS of about half of the total. VASP gets more DOS inside the spheres than ELK and our LAPW comes close to our corrected *s*-H DOS. Quantum Espresso (QE) gives the sum of the components equal to the total but ignores the large *d*-Ca component. The TB fit, which was performed very accurately using the Naval Research Laboratory TB (NRL-TB) method, had as input only our LAPW eigenvalues at $a = 6.4$ bohr, based on nonorthogonal *s*-, *p*-, *d*-Ca, and *s*-H orbitals and has an rms error of 0.024 Ry for seven bands fitted to 55 *k* points in the irreducible Brillouin zone. Taking into account that in the TB the sum of the ℓ components is equal to the total, a direct comparison with the LAPW projected ℓ components cannot be made, but the TB also gives the *d*-Ca as the largest component. At the outset the Ca contribution to λ is small and so the results in Ref. [28] turn out not to affect the basic conclusion regarding the dominance of hydrogen. The strong *d* character of the Ca DOS near E_f is well known. The reader can also see this in other Ca-H structures. See Ref. [31] for the NaCl and CsCl structures, and even for pure Ca the d-like contribution at E_f is strong [46]. Also see the 50-year-old paper by McCaffrey *et al.* [47].

The exact values of the angular momentum components of the CaH_6 DOS at ε_F are listed in Table I for different lattice parameters and corresponding pressures per one spin. These are also compared to the values from the other methods given in Appendix A, Table IX. It should be noted here that we have multiplied the ℓ components of the hydrogen DOS by a factor 1.5. We changed the multiplier to 1.4 and 1.6 and repeated the calculations for η. We have found that this results in a decrease of T_c by about 10 K for "1.4," and an increase by 10 K for "1.6," This is about the same change in T_c when the value of μ^* is changed from 0.13 to 0.10. Given the exponential form the Allen-Dynes equation for T_c, we find this reasonable. The independent calculation using VASP that we present in Appendix A finds the projected H DOS larger by about a factor of 1.4. The motivation for this correction comes from the realization that due to the geometry of the clathrate structure the LAPW calculation is done with very small muffin-tin spheres which results in unphysically small electron charge of about 0.5 electrons inside the hydrogen spheres. From Table I we observe that with increasing lattice constant, or decreasing pressure, $N(\varepsilon_F)$ is almost constant and has a noticeable increase of about 10%, only in the unstable region above $a = 6.8$ bohr. We also note that the *d*-Ca DOS is the largest ℓ-component DOS, even larger than the per site *s*-H DOS. Calculations using pseudopotentials (see Quan *et al.* [28]) often neglect the *d* states of Ca. Luckily, this omission does not lead to a serious error in the electron-phonon coupling due to the large force constant of the phonons in the Ca sites, as discussed later in the paper.

TABLE I. Density of states *N* and angular momentum components of the DOS at the Fermi level for CaH_6 as a function of the lattice constant and pressure, in states/(Ry spin). The hydrogen partial densities of states are presented per site and are multiplied by a factor 1.5 to correct for the small electron charge of approximately 0.5 electrons inside the muffin-tin spheres found in the LAPW calculations.

a	P		[states/(Ry spin)]			
(bohr)	(GPa)	$N(\varepsilon_F)$	*s*	*p*	*d*	*f*
6.0	353	2.496				
		Ca	0.014	0.127	0.344	0.023
		H	0.198	0.040	0.003	0.000
6.2	264	2.318				
		Ca	0.012	0.092	0.270	0.018
		H	0.188	0.032	0.002	0.000
6.4	197	2.318				
		Ca	0.011	0.070	0.240	0.015
		H	0.188	0.028	0.002	0.000
6.6	144	2.380				
		Ca	0.010	0.057	0.222	0.013
		H	0.191	0.025	0.001	0.000
6.8	105	2.468				
		Ca	0.009	0.047	0.210	0.011
		H	0.195	0.022	0.001	0.000
7.0	74	2.569	unstable			

To study the superconducting properties of this material we employ the classic McMillan equation (1) in Sec. II, which separates the electron and phonon contributions to the electron-phonon coupling. We first calculate the numerator of (1), the Hopfield parameter η defined by (2), the Gaspari-Gyorffy (GG) formula. The results are shown in Table II. We note that, in the range of pressures where CaH_6 is stable, both η(Ca) and η(H) increase with increasing pressure, and $\eta(\mathrm{H}) \gg \eta(\mathrm{Ca})$. In Table II we also list the values of $\langle I^2 \rangle$ and note that the Ca site shows an increase of 20% with pressure and the H sites show a similar increase with pressure. Since $N(\varepsilon_F)$ is almost constant with pressure we conclude that $\langle I^2 \rangle$ is the dominant parameter in the evaluation of η and indeed its hydrogen component. To provide further insights from the values of η shown in Table II we examine the GG formula (2) and

TABLE II. Hopfield parameter η (in eV/Å^2) and $\langle I^2\rangle$ [in (eV/Å)^2] for each atom type from (2) as a function of lattice constant a (in bohr) and pressure P (in GPa). The η values of H are multiplied by six to account for the six H sites. Results for only the stable volumes are shown.

		η		$\langle I^2\rangle$	
a	P	Ca	H	Ca	H
6.0	353	3.374	12.458	18.387	67.884
6.2	264	2.230	10.574	13.118	62.054
6.4	197	1.596	9.527	9.388	56.041
6.6	144	1.193	8.675	6.817	49.572
6.8	105	0.912	8.005	5.026	44.112

we note that the summation for $\ell = 0, 1, 2$ has three terms, which we call the *sp*, *pd*, and *df* channels. We have found the largest contributors to these channels are the Ca-*pd* channel and the H-*sp* channel for the H sites. In Table III we show the results for the lattice constant $a = 6.2$ bohr. We found similar results for the rest of the lattice constants/pressures indicating the strength of the Ca-*pd* and the H-*sp* channels. We also found that in the H-*sp* channel, which gives the strongest contribution to the value of η, the $\sin^2$ term and the DOS product term $v_\ell^j v_{\ell+1}^j$ contribute about equally.

Further analysis of the GG formula (2) reveals that it contains the sum of a product of three terms corresponding to $\ell = 0, 1, 2$ which we call channels *sp*, *pd*, and *df*. The three terms shown in Table IV are labeled $2(\ell+1)/N(\varepsilon_F)$, the phase shifts $\sin^2(\delta_\ell - \delta_{\ell+1})$, and the ratio of the partial DOS over the free scatterers. The following observations can be made from the values of the quantities listed in Table IV. The product of the three terms give the total η for each ℓ. The fourth column is dominated by the value of ℓ and the total DOS $N(\varepsilon_F)$. The fifth column is a sine function of the difference of phase shifts; it reaches its largest value for $\ell = 1$ (*pd* channel) in calcium, approaching 0.84 for the largest lattice constant. For the H sites the maximum remains about constant for the different lattice parameters at a value of about 0.3. Note that we have six H sites which means that H contribution is by far the largest. The sixth column is the ratio of the ℓ components of the DOS at ε_F over the free scatterers and reaches its largest value, well over 2, for $\ell = 2$. However the sixth column, which indicates the ℓ components of η, the most important parameter in our view, has the largest values for Ca in the *pd* channel ($\ell = 1$) and for H in the *sp* channel ($\ell = 0$).

We now consider the determination of the denominator of (1), the force constants $M\langle\omega^2\rangle$. We do this by interpolation/extrapolation of the phonon frequencies given by Quan *et al.* We list these in Table V.

TABLE III. Contributions to the Hopfield parameter η per atom for the three channels in units of eV/Å^2 respectively for lattice constant $a = 6.2$ bohr and $P = 264$ GPa.

	η-*sp*	η-*pd*	η-*df*	η-tot
Ca	0.314	1.070	0.845	2.230
H	10.548	0.025	0.000	10.574

TABLE IV. Tabulation of the values of the three multiplicative terms: $2(\ell+1)/N(\varepsilon_F)$, $\sin^2(\delta_\ell - \delta_{\ell+1})$, and the ratio of the DOS $v_\ell v_{\ell+1}$ for lattice constants $a = 6.2$, 6.4, 6.6, and 6.8 bohr corresponding to pressures $P = 264$, 197, 144, and 105 GPa respectively.

a (bohr)	P (GPa)	ℓ	$2(\ell+1)/N(\varepsilon_F)$ [per (eV spin)]	$\sin^2(\delta_\ell - \delta_{\ell+1})$	$v_\ell v_{\ell+1}$	η_ℓ (eV/Å^2)
			Ca site			
6.2	264	0	6.147	0.5034	0.1015	0.3141
		1	12.295	0.973	0.089	1.070
		2	18.442	0.174	0.263	0.846
			H site			
		0	6.147	0.2866	0.9979	1.758
		1	12.295	0.0004	0.8021	0.0042
		2	18.442	0.0000	2.3316	0.0000
			Ca site			
6.4	197	0	5.706	0.500	0.0732	0.209
		1	11.411	0.931	0.068	0.728
		2	17.117	0.149	0.259	0.660
			H site			
		0	5.706	0.302	0.919	1.585
		1	11.411	0.0004	0.747	0.003
		2	17.117	0.0000	2.236	0.0000
			Ca site			
6.6	144	0	5.171	0.496	0.057	0.147
		1	10.342	0.878	0.058	0.525
		2	15.513	0.126	0.267	0.522
			H site			
		0	5.171	0.318	0.878	1.443
		1	10.342	0.0004	0.737	0.003
		2	15.513	0.0000	2.297	0.0000
			Ca site			
6.8	105	0	4.654	0.492	0.047	0.107
		1	9.307	0.817	0.051	0.389
		2	13.961	0.107	0.279	0.416
			H site			
		0	4.654	0.333	0.858	1.332
		1	9.307	0.0003	0.733	0.002
		2	13.961	0.0000	2.039	0.0000

Using the Hopfield parameters η and the force constants $M\langle\omega^2\rangle$ listed in Tables III and V we can now compute the electron-phonon coupling constants $\lambda(j)$ for the two sites of CaH_6. The results are shown in Table VI, where we multiply the H components of λ by six to account for the number of hydrogen crystallographic sites. Table VI also lists the superconducting temperatures calculated by the Allen-Dynes formula (5) in Sec. II.

TABLE V. Averaged phonon frequencies for CaH_6 from Quan *et al.*

a (bohr)	P (GPa)	ω_2(Ca) (K)	ω_2(H) (K)	$\omega_{\log}$ (K)	$M\langle\omega^2\rangle$(Ca) (eV/Å^2)	$M\langle\omega^2\rangle$(H) (eV/Å^2)
6.0	353	524	2143	1476	19.549	8.222
6.2	264	452	1810	1357	14.546	5.866
6.4	197	418	1612	1276	12.440	4.653
6.6	144	382	1311	1044	10.389	3.077
6.8	105	351	1040	867	8.772	1.937

TABLE VI. Electron-phonon coupling constant λ, prefactors f_1 and f_2 of the Allen-Dynes equation, and superconducting temperature T_c. The Coulomb pseudopotential is set to $\mu^* = 0.13$.

a (bohr)	P (GPa)	λ(Ca)	λ(H)	λ_{tot}	f_1	f_2	T_c (K)
6.0	353	0.17	1.52	1.69	1.09	1.05	198
6.2	264	0.15	1.80	1.95	1.12	1.05	211
6.4	197	0.13	2.05	2.18	1.13	1.06	218
6.6	144	0.11	2.82	2.93	1.20	1.08	229
6.8	105	0.10	4.13	4.23	1.31	1.11	246

Given the fact that we have used the Allen-Dynes equation and not the Eliashberg equations, our results are consistent with those of Jeon *et al.* [29] including the decrease of λ and T_c with increasing pressure as shown in Table VI. In Jeon *et al.* no separation of λ into Ca and H contributions is made but the strong role of H is implied to be due to hardening of optical phonon modes. Also no values of the electronic densities of states at the Fermi level are given. On the other hand more details are given in the paper by Quan *et al.* [28], with which we agree on the conclusion that the λ(Ca) can be neglected as it is very small. A quantitative comparison of our results based on the decoupling of λ in the ratio of $\eta/M\langle\omega^2\rangle$ cannot be made due to the different way these authors applied the GG theory. As is the case with the other theoretical papers, our results agree with the experimental work [3–17].

IV. PREDICTIONS FOR EVEN HIGHER TRANSITION TEMPERATURES

Before we present our predictions we wish to bring attention to statements made by Quan *et al.* [28] and by Pickett [48] which argue that "Gaining an understanding of Hydrogen scattering I^2 is a current challenge but a realistic one and one that will be crucial in learning how to retain coupling over as many H branches as possible." Although these authors do not provide a detailed prescription for meeting this challenge they point towards the Allen and Dynes (AD) [37] discovery that, at least in ordinary superconductors, the McMillan-Hopfield parameter η determines T_c in the strong coupling limit. We present below a generalization of the AD strong coupling equation which seems to work well for the Ca-Sc-H system.

Earlier in this paper it was stated from Fig. 4 that a rigid band model would suggest that the DOS value at ε_F could be increased by replacing Ca atoms by Sc. In this section this idea is tested by the virtual crystal approximation (VCA). In the VCA we performed a standard LAPW calculation by replacing the atomic number Z of Ca by an average Z between Ca and Sc, and the number of valence electrons of Ca by the average of Ca and Sc valence electrons. The DOS calculated using the VCA are shown in Figs. 5 and 6 for $Ca_{0.5}Sc_{0.5}H_6$ and ScH_6 respectively. The rise of ε_F with addition of electrons is evident. Using these LAPW-VCA results for the total and angular momentum decomposed DOS at ε_F, and the corresponding potential energy functions $V(r)$, we have applied the GG theory and obtained the Hopfield parameters for the two sites. We recognize that the VCA may not be a reliable approximation to describe the electronic states of disordered

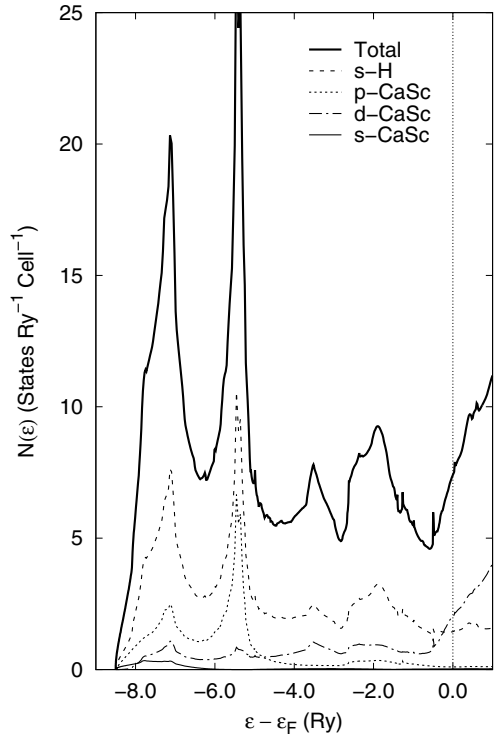

FIG. 5. Total and angular momentum decomposed DOS as a function of number of electrons for $Ca_{0.5}Sc_{0.5}H_6$ for $a = 6.4$ bohr. Note that ε_F is not at a minimum as it is in pure CaH_6.

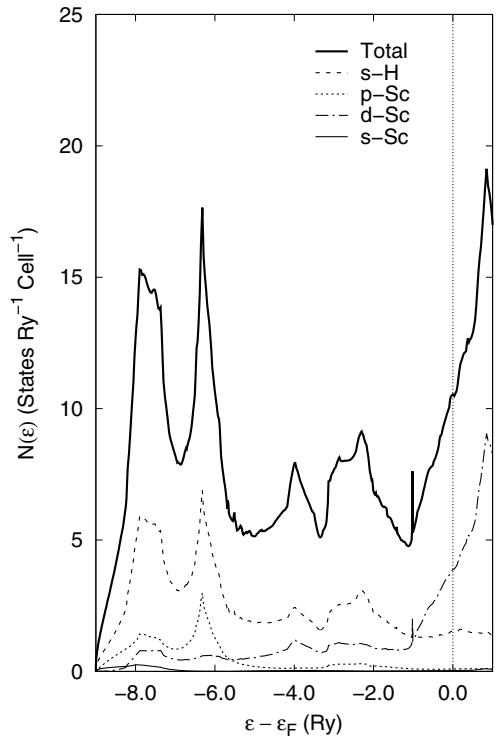

FIG. 6. Total and angular momentum decomposed DOS as a function of number of electrons for ScH_6 for $a = 6.4$ bohr. The DOS at ε_F is even higher than in the alloy.

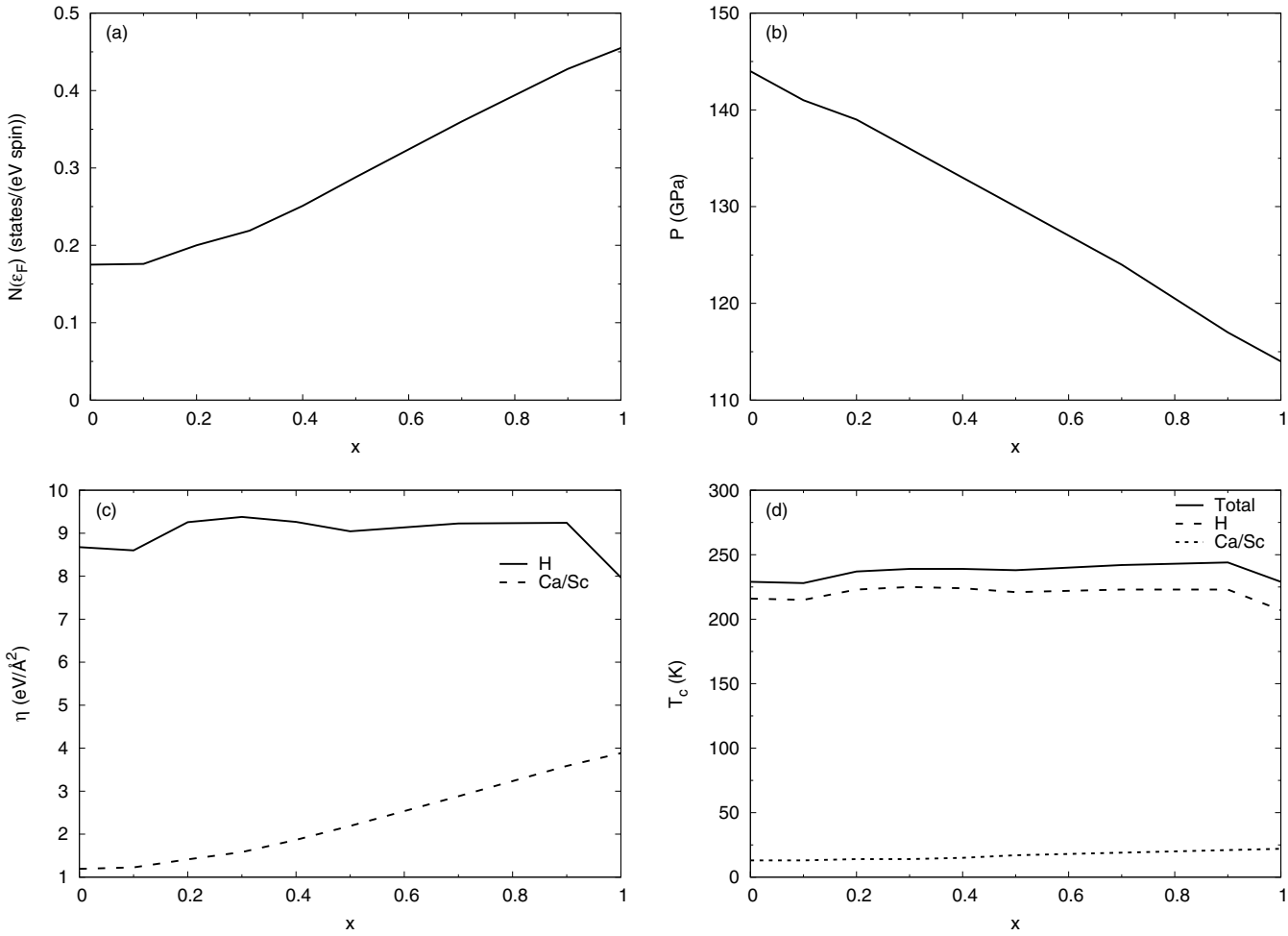

FIG. 7. Various quantities of the compound $Ca_{1-x}Sc_xH_6$ calculated in the virtual crystal approximation as a function of the scandium fraction x at the lattice constant $a = 6.6$ bohr. (a) The electronic density of states at the Fermi level. (b) The pressure. (c) η [Eq. (2)] for hydrogen (solid line) and $Ca_{1-x}Sc_x$ (dashed line). (d) The superconducting transition temperature. The solid line is the transition temperature, the dashed line is the hydrogen contribution, and the dotted line is the contribution from $Ca_{1-x}Sc_x$.

systems. However, in the presence of several unknown conditions, it is widely used as an indication for an expected complicated behavior. Thus, the use of the VCA brings a speculative element to our study but still the VCA results are indicative of what may happen by alloying Ca with Sc. Since we have already done a TB fit we could have tried a TB form of the coherent potential approximation (CPA), but the CPA does not link well with the GG formula that requires, in addition, the scattering phase shifts and the free scatterers which are not calculable within TB in an obvious way. In any case the spirit of our work is to show that Sc is potentially a reasonable candidate to increase T_c in $Ca_{1-x}Sc_xH_6$ which may motivate experiments and more detailed and accurate calculations. A recent paper on $ScCaH_{2n}$ by Shi *et al.* [49] includes calculations in other structures than the $Im3m$ that we used, which makes the comparison with our results only qualitative. In that sense we agree that addition of Sc can increase T_c, and so does the increase of the amount of H, which we bring up in the next section. We have followed Allen and Dynes [37], who found that, in the strong coupling (large λ) limit, the transition temperature T_c is proportional to $\sqrt{\eta/M}$ with the proportionality coefficient being a constant close to 0.15. We generalized their equation for a two atom system as follows:

$$T_c = A\left(\sqrt{\frac{\eta_{\mathrm{Ca}}}{M_{\mathrm{Ca}}}} + \sqrt{\frac{\eta_{\mathrm{H}}}{M_{\mathrm{H}}}}\right). \tag{10}$$

Here η is in units of eV/Å^2 and M is the mass number i.e., 1 for H and about 40 for Ca and 45 for Sc. The numerical factor A is determined from our results for CaH_6 where we have already calculated T_c using the phonon frequencies of Quan *et al.* [28] for various values of the pressure (or the lattice constant). As a result A depends strongly on η in such a way that T_c is a decreasing function of η in agreement with Eq. (12) below. It should be noted that for the calculations and the ongoing discussion using Eq. (10) for the alloy $Ca_{1-x}Sc_xH_6$ the phonon frequencies are not needed as long as we stay at the strong coupling limit. This makes this approach computationally efficient for searches of new superconductors. Our calculations of T_c and related quantities as a function of the concentration x of Sc are summarized in Fig. 7.

The detailed results for the parameters influencing superconductivity in the VCA calculations for $Ca_{0.5}Sc_{0.5}H_6$ and

TABLE VII. Parameters used for the determination of T_c for the Ca-Sc alloys and ScH_6 to be compared with those in Table VI for CaH_6. ScH_6 has imaginary phonon frequencies for $a > 6.6$ bohr and so is unstable at lower pressures. We estimate that $Ca_{1-x}Sc_xH_6$ becomes unstable for a in the range 6.6–6.8 bohr.

a (bohr)	P (GPa)	$\eta_{\text{Ca-Sc}}$ (eV/Å^2)	η_{H} (eV/Å^2)	$N(\varepsilon_F)$ [states/(eV spin)]	T_c (K)
			$Ca_{0.5}Sc_{0.5}H_6$		
6.0	332	4.485	11.457	0.261	192
6.2	247	3.517	10.336	0.272	212
6.4	181	2.798	9.784	0.285	225
6.6	130	2.191	9.043	0.288	238
			ScH_6		
6.0	310	6.299	10.488	0.356	187
6.2	225	5.332	9.873	0.387	211
6.4	161	4.423	8.749	0.414	217
6.6	114	3.886	7.971	0.455	229

for ScH_6 are shown in Table VII. We note that $N(\varepsilon_F)$ and $\eta_{\text{Ca-Sc}}$ (shown in Fig. 7) are both larger than in pure CaH_6. This increase comes mostly from the d states of Sc, which is not surprising. On the other hand the results for ηH are mixed while T_c increases up to the Sc concentration $x = 0.9$ and then it drops towards the ScH_6 end. So as shown in Fig. 7 the effect of the increased Ca(Sc) d-like character of the states at ε_F is a corresponding strong increase of $\eta_{\text{Ca-Sc}}$ and a modest increase of η_{H} $Ca_{1-x}Sc_xH_6$, which is enough to raise T_c by about 10 K near $x = 0.4$. Figure 7 also shows the splitting [allowed by Eq. (10)] in the Ca-Sc and H components which show the suspected result that the H contribution is much stronger but the Ca-Sc contribution is not negligible. Inspecting Fig. 7 we see that $N(\varepsilon_f)$ is monotonically increasing with the Sc concentration x, which is consistent with the rigid band picture. However, the dependence of T_c on x is more complicated because T_c depends on η. So $\eta_{\text{Ca-Sc}}$ increases with x while η_{H} decreases with x. This opposite variation of η is due to the fact that at the CaH_6 end at ε_f the H states dominate but as we add Sc the contribution of the d states becomes larger and the H states become less dominant as ε_f moves up.

At this point we wish to comment on the dependence of T_c versus pressure. The calculations of Quan *et al.* [28], from which we are using the phonon frequencies, as well as the results of Jeon *et al.* [29] with which we are comparing in Fig. 8, show that T_c increases with decreasing pressure. We agree with these calculations but we all seem to have a disagreement with Wang *et al.* [25] However, the calculations were done assuming the $Im\bar{3}m$ crystal symmetry. It is not entirely clear that the measurements do not involve mixed phases. We also want to add that, for all concentrations x, our calculations maintain the decrease of T_c with increasing pressure, not to be confused with the enhancement of T_c with increasing x. This is more clearly shown in Tables X, XI, XII, and XIII in Appendix B.

We have also performed similar calculations for CaH_3 and CaH_{10} in the $Im\bar{3}m$ and $Fm\bar{3}m$ structures, respectively, to examine the possibility of finding higher transition temperatures. We recognize that the structures we assumed are not among those identified in Refs. [25,49,50]. Our claim is that an increase of the H content increases T_c in CaH_{10}, which is widely believed about these materials, and it is probably the case independent of crystal structure. Our results are given in Table VIII. In this table we note that the force constants $M\langle\omega^2\rangle$ used to obtain the corresponding λ are assumed to be the same as in CaH_6. Using η(H) as an indicator to predict high T_c, we observe very high T_c in CaH_{10}. It is also interesting to notice that high T_c values found in CaH_{10} correspond to lower pressures than in CaH_6.

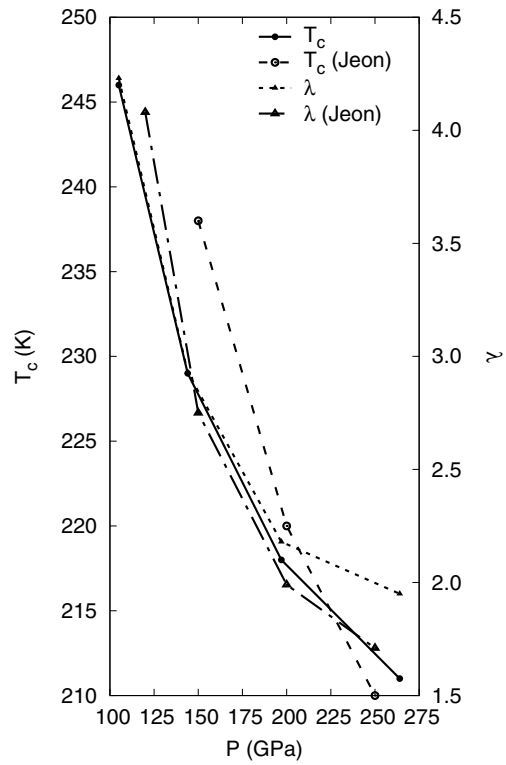

FIG. 8. CaH_6 superconducting transition temperature T_c (circles) and λ_{tot} (triangles) versus pressure using the values from Table VI (solid symbols) and comparing to the predictions of Jeon *et al.* [29] (open symbols).

V. THE RELATIVE IMPORTANCE OF THE PARAMETERS η AND λ

From Table II we can see that $d\eta/dP > 0$ and from Table V we find $d\kappa/dP > 0$, where $\kappa = M\langle\omega^2\rangle$ is the force constant. However, κ grows faster than η with increasing pressure. As a result, since the electron-phonon parameter λ is the ratio η/k, it follows that $d\lambda/dP < 0$, as indicated in Fig. 9 and Table VI. It turns out that in the present case the critical temperature T_c follows the same behavior versus pressure as λ, i.e., $dT_c/dP < 0$. This lets us write

$$\frac{d\lambda}{dT_c} = \left(\frac{d\lambda}{dP}\right) \times \left(\frac{dP}{dT_c}\right) = (-) \times (-) > 0 \tag{11}$$

and

$$\frac{d\eta}{dT_c} = \left(\frac{d\eta}{dP}\right) \times \left(\frac{dP}{dT_c}\right) = (+) \times (-) < 0, \tag{12}$$

TABLE VIII. Parameters used for the determination of T_c for CaH_3 and CaH_{10}.

a (bohr)	P (GPa)	λ (Ca)	λ (H)	λ_{tot}	T_c (K)	η (Ca) (eV/Å^2)	η (H) (eV/Å^2)	$N(\varepsilon_F)$ [states/(eV spin)]
				CaH_3				
5.8	265	0.448	0.716	1.164	111	6.519	4.197	0.306
6.0	197	0.407	0.827	1.234	114	5.059	3.847	0.265
6.2	146	0.421	1.212	1.633	133	4.371	3.729	0.271
6.4	108	0.294	0.773	1.067	91	3.659	3.595	0.286
				CaH_{10}				
8.9	184	0.100	2.61	2.71	244	1.192	10.742	0.312
9.0	167	0.099	2.92	3.02	251	1.098	10.426	0.317
9.2	133	0.095	3.76	3.86	263	0.931	9.849	0.328
9.4	106	0.100	4.87	4.97	275	0.885	9.536	0.347

as seen in Tables II and VI.

The above analysis explains why λ is a better indicator of high T_c than η, at least for CaH_6 and LaH_{10}, as shown in Figs. 9 and 10. This is rather surprising, since we are in the strong coupling limit and as a result we expect to reach the Allen-Dynes limiting relation

$$T_c \propto \sqrt{\frac{\eta}{M}}. \tag{13}$$

Instead T_c is a decreasing function of η and follows more or less λ and not η. A possible explanation for this anomaly is the strong stiffening of the force constant κ, due to the extreme high pressures, which prevents the limiting value of T_c from becoming a function of only η. Therefore the balancing act between η and k for obtaining high values of λ and hence T_c remains the same in the high-temperature superconducting hydrides as in the ordinary temperature superconductors. Although the limiting value of T_c cannot be reached in the hydrides, nevertheless, as discussed in the previous section, Eq. (10) with A being an adjustable parameter seems to be a reasonable approximation for the high pressure hydrides. However, still η plays an important role because in order to reach high T_c one needs values of λ of the order of 2 and

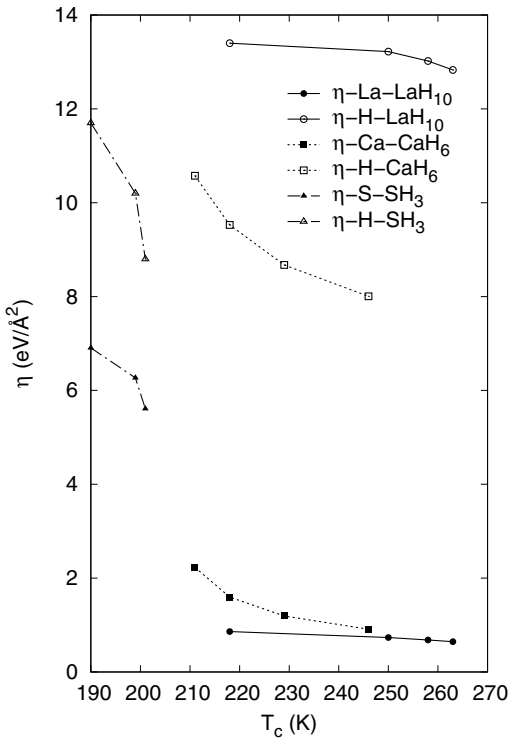

FIG. 9. Total electronic contribution η [Eq. (2)] as a function of the superconducting transition temperature, decomposed by the angular momentum. The solid line is for LaH_{10}, the dashed line for CaH_6, and the dotted line for SH_3. The solid symbols represent the cation contribution, while the open symbols represent the anions (H).

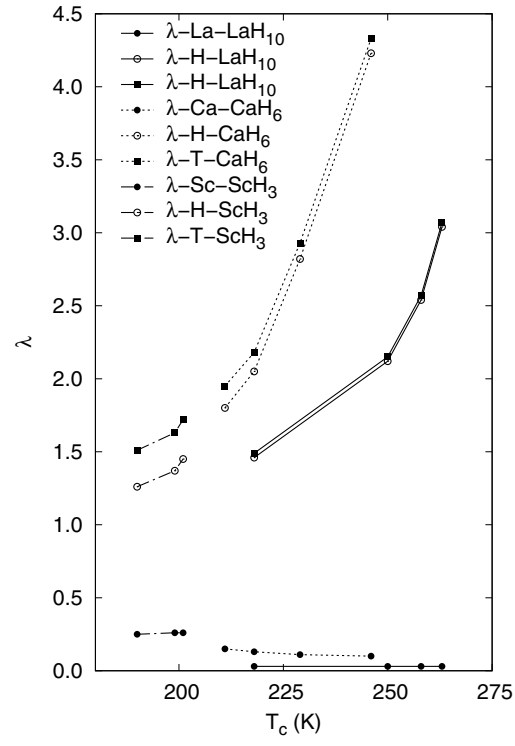

FIG. 10. Electron-phonon coupling λ [Eq. (1)] as a function of the superconducting transition temperature for LaH_{10} [30] (solid lines), CaH_6 (dotted-lines), and SH_3 [16] (dash-dot lines). The cation contribution to λ is represented by a solid circle, the open circles are the anion (hydrogen) contribution, and the solid squares represent the total value.

TABLE IX. Decomposed and total density of states [states/(eV two-spins)] for CaH_6 at $a = 6.4$ bohr using a variety of electronic structure methods. The LAPW muffin-tin radius is 1.8 bohr for calcium and 1.0 bohr for hydrogen. ELK uses the default muffin-tin radius, 2.4 bohr, for calcium. The program decreases the muffin-tin radius of hydrogen from the default value of 1.4 to 1.1 bohr. "Total" is the total DOS at the Fermi level, while "Inside" is the sum of the DOS inside the spheres.

DOS	LAPW	VASP	ELK	QE	TB fit
Total	0.341	0.354	0.311	0.367	0.310
H(s)	0.0184×6	0.0220×6	0.0187×6	0.0445×6	0.2405(6H)
H(p)	0.0027×6	0.0046×6	0.0026×6		
Ca(s)	0.0016	0.0039	0.0024	0.0738	0.0036
Ca(p)	0.0104	0.0135	0.0115	0.0347	0.0068
Ca(d)	0.0353	0.0666	0.0324		0.0592
Inside	0.1739	0.2436	0.1741	0.376	0.310

TABLE X. $a = 6.0$ bohr, $A = 51.84$.

x	a (bohr)	P (GPa)	$N(\varepsilon_F)$ [states/(eV spin)]	$\eta_{Ca_{1-x}Sc_x}$ (eV/Å^2)	η_{H} (eV/Å^2)	$I^2_{Ca_{1-x}Sc_x}$ [(eV/Å)^2]	I^2_{H} [(eV/Å)^2]	T_c ($Ca_{1-x}Sc_x$) (K)	T_c (H) (K)	T_c (K)
0.0	6.0	353	0.184	3.374	12.458	18.387	67.884	15	183	198
0.1	6.0	351	0.197	3.548	12.677	18.010	64.350	15	185	200
0.2	6.0	346	0.209	3.705	12.412	17.727	59.388	16	183	198
0.3	6.0	342	0.229	4.015	12.086	17.533	52.777	16	180	196
0.4	6.0	337	0.248	4.285	11.695	17.278	47.157	17	177	194
0.5	6.0	332	0.261	4.485	11.457	17.184	43.897	17	175	192
0.7	6.0	325	0.297	5.113	10.941	17.215	36.838	18	171	189
0.9	6.0	314	0.340	5.941	10.563	17.474	31.068	19	168	187
1.0	6.0	310	0.356	6.299	10.488	17.694	29.461	19	168	187

TABLE XI. $a = 6.2$ bohr, $A = 60.5$.

x	a (bohr)	P (GPa)	$N(\varepsilon_F)$ [states/(eV spin)]	$\eta_{Ca_{1-x}Sc_x}$ (eV/Å^2)	η_{H} (eV/Å^2)	$I^2_{Ca_{1-x}Sc_x}$ [(eV/Å)^2]	I^2_{H} [(eV/Å)^2]	T_c ($Ca_{1-x}Sc_x$) (K)	T_c (H) (K)	T_c (K)
0.0	6.2	264	0.170	2.230	10.574	13.118	62.200	14	197	211
0.1	6.2	262	0.185	2.421	11.016	13.086	59.546	15	201	216
0.2	6.2	257	0.204	2.629	11.200	12.887	54.902	15	202	217
0.3	6.2	253	0.228	2.926	11.090	12.833	48.640	16	201	217
0.4	6.2	250	0.250	3.214	10.663	12.856	42.652	17	198	215
0.5	6.2	247	0.272	3.517	10.336	12.930	38.000	17	195	212
0.7	6.2	239	0.312	4.098	9.956	13.135	31.910	19	191	210
0.9	6.2	229	0.366	4.981	9.924	10.571	27.115	20	191	211
1.0	6.2	225	0.387	5.332	9.873	13.778	25.512	21	190	211

TABLE XII. $a = 6.4$ bohr, $A = 66.339$.

x	a (bohr)	P (GPa)	$N(\varepsilon_F)$ [states/(eV spin)]	$\eta_{Ca_{1-x}Sc_x}$ (eV/Å^2)	η_{H} (eV/Å^2)	$I^2_{Ca_{1-x}Sc_x}$ [(eV/Å)^2]	I^2_{H} [(eV/Å)^2]	T_c ($Ca_{1-x}Sc_x$) (K)	T_c (H) (K)	T_c (K)
0.0	6.4	197	0.170	1.596	9.527	9.388	56.041	13	205	218
0.1	6.4	193	0.201	1.868	10.680	9.293	53.134	14	217	231
0.2	6.4	190	0.198	1.872	10.128	9.455	51.152	14	211	225
0.3	6.4	187	0.227	2.150	10.343	9.471	45.564	15	213	228
0.4	6.4	184	0.244	2.374	9.909	9.730	40.611	16	209	225
0.5	6.4	181	0.285	2.798	9.784	9.618	34.330	17	208	225
0.7	6.4	173	0.332	3.400	9.537	10.241	28.726	19	205	223
0.9	6.4	165	0.399	4.218	9.352	10.571	23.439	20	203	223
1.0	6.4	161	0.414	4.423	8.749	10.684	21.133	21	196	217

above, which means that η has to be about two times larger than the force constant. Indeed, this condition is satisfied in CaH_6 as can be seen by comparing the η and $M\langle\omega^2\rangle$ values for lattice constants of $a = 6.2$ to 6.8 bohr given in Tables II and V. Therefore, η is a reasonable predictor of high-temperature superconductivity when it reaches values over 10 eV/Å^2, despite the delicate interplay with the force constant. In that case η becomes important in a search for new high-temperature superconductors before considering doing the computationally demanding phonon calculations. In the latter, along the lines of increasing T_c or reducing the pressure range, the stability issue is of great current interest. For example, the instability for lower pressures, as deduced from Fig. 2, is due to both the transverse acoustic branch(determined from metal oscillations) and the lower optic branch of hydrogen both at the symmetry point H of the Brillouin zone. Thus, the instability, which is due to the hydrogens losing their metallic character seems to depend on the metallic component as well. This is not surprising since the latter plays a decisive role in stabilizing the metallic character of the hydrogens in the first place.

VI. CONCLUSIONS

We have performed LAPW band structure calculations to apply the Gaspari-Gyorffy theory for determining the Hopfield parameter η. We have combined these with published results of the phonon frequencies to calculate the electron-phonon coupling and the superconducting transition temperature T_c for CaH_6. The results for η, accounting for the six hydrogen sites in the structure, make the H contribution about 9 times stronger than that from Ca. Due to the larger force constant of Ca than H, which makes the λ(Ca) small, this conclusion of the dominance of the hydrogen sites is retained and even strengthened. Thus, the acoustic modes associated with Ca contribute 7% to the total value of λ, in contrast to the optic modes associated with hydrogen which contribute 93% for the H. This is reminiscent of LaH_{10} where La has only a 2% contribution. Our results are in good agreement regarding the high values of T_c obtained by experiment and other theoretical works. So the notion that the so-called superhydrides such as SH_3 and LaH_{10} are metallic hydrogen superconductors is supported by one more example, CaH_6. A detailed analysis of the various terms of the GG formula is given to clarify the relative importance of these terms which may lead to discovering how to raise the value of η at low pressures and therefore help in the search of room temperature superconductors. We also present calculations for $Ca_{1-x}Sc_xH_6$ using the VCA which predict that alloying Ca with Sc shows enhancement of T_c due to the substantial increase of the parameters η in the strong coupling limit. In addition, we performed calculations for CaH_{10} where the increase of the hydrogen content in the Ca-H system results in an increase of the superconducting temperature provided that CaH_{10} can form a high pressure $Fm\bar{3}m$ structure. From the findings of this work we conclude that λ and the competing η and κ are all important in investigating superconductivity in the hydrides. The λ is directly controlling T_c via the Allen-Dynes equation. However, T_c values exceeding 200 K require values of $\lambda = 2$ and above. Since $\lambda = \eta/\kappa$ it follows that $\eta > 2\kappa$. This means that η plays an important role through its interplay with κ. We propose that in the search for high T_c materials values of η exceeding 10 eV/Å^2 is essential and should be the first step in the search before proceeding with the computationally expensive calculations of the phonons.

ACKNOWLEDGMENT

We thank W. E. Pickett for a useful email communication.

APPENDIX A: CONTRIBUTIONS TO THE DENSITY OF STATES AT THE FERMI LEVEL

Table IX lists the total density of states at ε_F together with its angular momentum components. This is a comparison between the results given by our LAPW code and those we calculated using the VASP, ELK and Quantum Espresso (QE) codes as well as those found by the NRL-TB fit. The agreement is generally good except that the QE misses the strong contribution of the Ca d-states as discussed in Sec. III.

APPENDIX B: CONTRIBUTIONS TO T_c

Tables X–XIII show the density of states at the Fermi level, η (2), the electron-ion matrix elements I^2, and the superconducting transition temperature T_c for $Ca_{1-x}Sc_xH_6$ as a function of the lattice constant and scandium concentration x. The contributions to T_c from Ca/Sc and H are computed using Eq. (10) with the value of A given for each lattice constant.

TABLE XIII. $a = 6.6$ bohr, $A = 73.45$.

x	a (bohr)	P (GPa)	$N(\varepsilon_F)$ [states/(eV spin)]	$\eta_{Ca_{1-x}Sc_x}$ (eV/Å^2)	η_H (eV/Å^2)	$I^2_{Ca_{1-x}Sc_x}$ [(eV/Å)^2]	I^2_H [(eV/Å)^2]	T_c ($Ca_{1-x}Sc_x$) (K)	T_c (H) (K)	T_c (K)
0.0	6.6	144	0.175	1.193	8.675	6.817	49.572	13	216	229
0.1	6.6	141	0.176	1.227	8.601	6.972	48.869	13	215	228
0.2	6.6	139	0.200	1.414	9.257	7.070	46.285	14	223	237
0.3	6.6	136	0.219	1.584	9.378	7.233	42.822	14	225	239
0.4	6.6	133	0.251	1.867	9.263	7.438	36.904	15	224	239
0.5	6.6	130	0.288	2.191	9.043	7.608	31.399	17	221	238
0.7	6.6	124	0.360	2.881	9.226	8.003	25.628	19	223	242
0.9	6.6	117	0.428	3.586	9.242	8.379	21.593	21	223	244
1.0	6.6	114	0.455	3.886	7.971	8.541	17.519	22	207	229

[1] D. Duan, Y. Liu, F. Tian, D. Li, X. Huang, Z. Zhao, H. Yu, B. Liu, W. Tian, and T. Cui, Pressure-induced metallization of dense $(H_2S)_2H_2$ with high-T_c superconductivity, Sci. Rep. **4**, 30 (2014).

[2] D. Hicks, M. J. Mehl, E. Gossett, C. Toher, O. Levy, R. M. Hanson, G. Hart, and S. Curtarolo, The AFLOW library of crystallographic prototypes: Part 2, Comput. Mater. Sci. **161**, S1 (2019).

[3] A. P. Drozdov, M. I. Eremets, I. A. Troyan, V. Ksenofontov, and S. I. Shylin, Conventional superconductivity at 203 kelvin at high pressures in the sulfur hydride system, Nature (London) **525**, 73 (2015).

[4] F. Fan, D. A. Papaconstantopoulos, M. J. Mehl, and B. M. Klein, High-temperature superconductivity at high pressures for $H_3Si_xP_{1-x}$, $H_3P_xS_{1-x}$, and $H_3Cl_xS_{1-x}$, J. Phys. Chem. Solids **99**, 105 (2016).

[5] J. A. Flores-Livas, A. Sanna, and E. K. Gross, High temperature superconductivity in sulfur and selenium hydrides at high pressure, Eur. Phys. J. B **89**, 63 (2016).

[6] Y. Ge, F. Zhang, and Y. Yao, First-principles demonstration of superconductivity at 280 K in hydrogen sulfide with low phosphorus substitution, Phys. Rev. B **93**, 224513 (2016).

[7] H. Liu, I. I. Naumov, R. Hoffmann, N. W. Ashcroft, and R. J. Hemley, Potential high T_c superconducting lanthanum and yttrium hydrides at high pressure, Proc. Natl. Acad. Sci. USA **114**, 6990 (2017).

[8] D. A. Papaconstantopoulos, M. J. Mehl, and H. Liu, Stability and high-temperature superconductivity in hydrogenated chlorine, Quantum Stud. Math. Found. **5**, 23 (2018).

[9] D. A. Papaconstantopoulos, Possible high-temperature superconductivity in hygrogenated fluorine, Novel Supercond. Mater. **3**, 29 (2017).

[10] S. Zhang, Y. Wang, J. Zhang, H. Liu, X. Zhong, H. F. Song, G. Yang, L. Zhang, and Y. Ma, Phase diagram and high-temperature superconductivity of compressed selenium hydrides, Sci. Rep. **5**, 15433 (2015).

[11] X. Zhong, H. Wang, J. Zhang, H. Liu, S. Zhang, H. F. Song, G. Yang, L. Zhang, and Y. Ma, Tellurium hydrides at high pressures: High-temperature superconductors, Phys. Rev. Lett. **116**, 057002 (2016).

[12] C. Heil and L. Boeri, Influence of bonding on superconductivity in high-pressure hydrides, Phys. Rev. B **92**, 060508(R) (2015).

[13] M. Mahdi Davari Esfahani, Z. Wang, A. R. Oganov, H. Dong, Q. Zhu, S. Wang, M. S. Rakitin, and X.-F. Zhou, Superconductivity of novel tin hydrides (Sn_nH_m) under pressure, Sci. Rep. **6**, 22873 (2016).

[14] T. Matsuoka, M. Hishida, K. Kuno, N. Hirao, Y. Ohishi, S. Sasaki, K. Takahama, and K. Shimizu, Superconductivity of platinum hydride, Phys. Rev. B **99**, 144511 (2019).

[15] A. P. Drozdov, P. P. Kong, V. S. Minkov, S. P. Besedin, M. Kuzovnikov, S. Mozaffari, L. Balicas, F. F. Balakirev, D. E. Graf, V. B. Prakapenka, E. Greenberg, D. A. Knyazev, M. Tkacz, and M. I. Eremets, Superconductivity at 250 K in lanthanum hydride under high pressures, Nature (London) **569**, 528 (2019).

[16] D. A. Papaconstantopoulos, B. M. Klein, M. J. Mehl, and W. E. Pickett, Cubic H_3S around 200 GPa: An atomic hydrogen superconductor stabilized by sulfur, Phys. Rev. B **91**, 184511 (2015).

[17] F. Peng, Y. Sun, C. J. Pickard, R. J. Needs, Q. Wu, and Y. Ma, Hydrogen clathrate structures in rare earth hydrides at high pressures: Possible route to room-temperature superconductivity, Phys. Rev. Lett. **119**, 107001 (2017).

[18] M. Somayazulu, M. Ahart, A. K. Mishra, Z. M. Geballe, M. Baldini, Y. Meng, V. V. Struzhkin, and R. J. Hemley, Evidence for superconductivity above 260 K in lanthanum superhydride at megabar pressures, Phys. Rev. Lett. **122**, 027001 (2019).

[19] E. Wigner and H. B. Huntington, On the possibility of a metallic modification of hydrogen, J. Chem. Phys. **3**, 764 (1935).

[20] N. W. Ashcroft, Metallic hydrogen: A high-temperature superconductor? Phys. Rev. Lett. **21**, 1748 (1968).

[21] D. A. Papaconstantopoulos and B. M. Klein, Electron-phonon interaction and superconductivity in metallic hydrogen, Ferroelectrics **16**, 307 (1977).

[22] G. D. Gaspari and B. L. Gyorffy, Electron-phonon interactions, *d* resonances, and superconductivity in transition metals, Phys. Rev. Lett. **28**, 801 (1972).

[23] J. M. McMahon, M. A. Morales, C. Pierleoni, and D. M. Ceperley, The properties of hydrogen and helium under extreme conditions, Rev. Mod. Phys. **84**, 1607 (2012).

[24] W. Pickett and M. Eremets, The quest for room-temperature superconductivity in hydrides, Phys. Today **72**(5), 52 (2019).

[25] H. Wang, J. S. Tse, K. Tanaka, and Y. Ma, Superconductive sodalite-like clathrate calcium hydride at high pressures, Proc. Natl. Acad. Sci. USA **109**, 6463 (2012).

[26] L. Ma, K. Wang, Y. Xie, X. Yang, Y. Wang, M. Zhou, H. Liu, X. Yu, Y. Zhao, H. Wang, G. Liu, and Y. Ma, High-temperature superconducting phase in clathrate calcium hydride CaH_6 up to 215 K at a pressure of 172 GPa, Phys. Rev. Lett. **128**, 167001 (2022).

[27] Z. Li, X. He, C. Zhang, X. Wang, S. Zhang, Y. Jia, S. Feng, K. Lu, J. Zhao, J. Zhang, B. Min, Y. Long, R. Yu, L. Wang, M. Ye, Z. Zhang, V. Prakapenka, S. Chariton, P. A. Ginsberg, J. Bass *et al.*, Superconductivity above 200 K discovered in superhydrides of calcium, Nat. Commun. **13**, 2863 (2022).

[28] Y. Quan, S. S. Ghosh, and W. E. Pickett, Compressed hydrides as metallic hydrogen superconductors, Phys. Rev. B **100**, 184505 (2019).

[29] H. Jeon, C. Wang, S. Liu, J. M. Bok, Y. Bang, and J.-H. Cho, Electron-phonon coupling and superconductivity in an alkaline earth hydride CaH_6 at high pressures, New J. Phys. **24**, 083048 (2022).

[30] D. A. Papaconstantopoulos, M. J. Mehl, and P.-H. Chang, High-temperature superconductivity in LaH_{10}, Phys. Rev. B **101**, 060506(R) (2020).

[31] D. Papaconstantopoulos, *Band Structure of Cubic Hydrides* (Springer, Cham, 2023).

[32] D. J. Singh, *Planewaves, Pseudopotentials, and the LAPW Method* (Kluwer Academic, Boston, 1994).

[33] O. K. Andersen, Linear methods in band theory, Phys. Rev. B **12**, 3060 (1975).

[34] L. Hedin and B. I. Lundqvist, Explicit local exchange-correlation potentials, J. Phys. C **4**, 2064 (1971).

[35] W. L. McMillan, Transition temperature of strong-coupled superconductor, Phys. Rev. **167**, 331 (1968).

[36] J. J. Hopfield, Angular momentum and transition-metal superconductivity, Phys. Rev. **186**, 443 (1969).

[37] P. B. Allen and R. C. Dynes, Transition temperature of strong-coupled superconductors reanalyzed, Phys. Rev. B **12**, 905 (1975).

[38] B. M. Klein and D. A. Papaconstantopoulos, On calculating the electron-phonon mass enhancement lambda for compounds, J. Phys. F **6**, 1135 (1976).

[39] G. Kresse and J. Hafner, *Ab initio* molecular dynamics for liquid metals, Phys. Rev. B **47**, 558 (1993).

[40] G. Kresse and J. Hafner, *Ab initio* molecular-dynamics simulation of the liquid-metal-amorphous-semiconductor transition in germanium, Phys. Rev. B **49**, 14251 (1994).

[41] G. Kresse and J. Furthmüller, Efficiency of *ab-initio* total energy calculations for metals and semiconductors using a plane-wave basis set, Comput. Mater. Sci. **6**, 15 (1996).

[42] G. Kresse and J. Furthmüller, Efficient iterative schemes for *ab initio* total-energy calculations using a plane-wave basis set, Phys. Rev. B **54**, 11169 (1996).

[43] S. Curtarolo, W. Setyawan, G. L. W. Hart, M. Jahnátek, R. V. Chepulskii, R. H. Taylor, S. Wang, J. Xue, K. Yang, O. Levy, M. J. Mehl, H. T. Stokes, D. O. Demchenko, and D. Morgan, AFLOW: An automatic framework for high-throughput materials discovery, Comput. Mater. Sci. **58**, 218 (2012).

[44] C. Toher, C. Oses, D. Hicks, E. Gossett, F. Rose, P. Nath, D. Usanmaz, D. C. Ford, E. Perim, C. E. Calderon, J. J. Plata, Y. Lederer, M. Jahnátek, W. Setyawan, S. Wang, J. Xue, K. Rasch, R. V. Chepulskii, R. H. Taylor, G. Gomez *et al.*, The AFLOW fleet for materials discovery, in *Handbook of Materials Modeling*, edited by W. Andreoni and S. Yip (Springer International, Cham, 2018), pp. 1–28.

[45] C. Oses, C. Toher, and S. Curtarolo, Data-driven design of inorganic materials with the automatic flow framework for materials discovery, MRS Bull. **43**, 670 (2018).

[46] D. A. Papaconstantopoulos, *Handbook of the Band Structure of Elemental Solids* (Springer, New York, 2015).

[47] J. W. McCaffrey, J. R. Anderson, and D. A. Papaconstantopoulos, Electronic structure of calcium as a function of the lattice constant, Phys. Rev. B **7**, 674 (1973).

[48] W. E. Pickett, Colloquium: Room temperature superconductivity: The roles of theory and materials design, Rev. Mod. Phys. **95**, 021001 (2023).

[49] L.-T. Shi, Y.-K. Wei, A.-K. Liang, R. Turnbull, C. Cheng, X.-R. Chen, and G.-F. Ji, Prediction of pressure-induced superconductivity in the novel ternary system $ScCaH_{2n}$ ($n = 1$–6), J. Mater. Chem. C **9**, 7284 (2021).

[50] Z. Shao, D. Duan, Y. Ma, H. Yu, H. Song, H. Xie, D. Li, F. Tian, B. Liu, and T. Cui, Unique phase diagram and superconductivity of calcium hydrides at high pressures, Inorg. Chem. **58**, 2258 (2019).